

# The excitation of inertial-acoustic waves through turbulent fluctuations in accretion discs I: WKBJ theory

T. Heinemann<sup>1</sup> and J. C. B. Papaloizou<sup>1</sup>

<sup>1</sup>*University of Cambridge, Wilberforce Road, Cambridge CB3 0WA*

3 May 2022

## ABSTRACT

We study and elucidate the mechanism of inertial-acoustic wave excitation in a differentially rotating flow with turbulence which could result from the magneto-rotational instability. We formulate a set of wave equations with sources that are only non-zero in the presence of turbulent fluctuations. We solve these in a shearing box domain, subject to the boundary conditions of periodicity in shearing coordinates, using a WKBJ method. It is found that, for a particular azimuthal wave length, the wave excitation occurs through a sequence of regularly spaced swings during which the wave changes from leading to trailing form. This is a generic process that is expected to occur in shearing discs with turbulence. Trailing waves of equal amplitude propagating in opposite directions are produced both of which produce an outward angular momentum flow that we give expressions for as functions of the disc parameters and azimuthal wave length. By solving the wave amplitude equations numerically we justify the WKBJ approach for a Keplerian rotation law for all parameter regimes of interest. In order to quantify the wave excitation approach completely the important wave source terms need to be specified. Assuming conditions of weak non-linearity, these can be identified and are associated with a quantity related to the potential vorticity, being the only survivors in the linear regime. Under the additional assumption that the source has a flat power spectrum at long azimuthal wave lengths, the optimal azimuthal wave length produced is found to be determined solely by the WKBJ response and is estimated to be  $2\pi H$ , with  $H$  being the putative disc scale height. In a following paper by Heinemann & Papaloizou, we perform direct three dimensional simulations and compare results manifesting the wave excitation process and its source with the assumptions made and the theory developed here in detail, finding excellent agreement.

## 1 INTRODUCTION

Accretion discs are ubiquitous in astrophysics, occurring in close binary systems, active galactic nuclei and around protostars (see e.g. Papaloizou & Lin 1995; Lin & Papaloizou 1996, for reviews). Ever since their importance was first realized it has been clear that some form of turbulence is necessary to provide the anomalous angular momentum transport implied by observed luminosities and inferred accretion rates. This has usually been parametrised using the Shakura & Syunyaev (1973)  $\alpha$  parametrisation.

The most likely source of the turbulence is through the magneto-rotational instability (MRI) (see Balbus & Hawley 1991, 1998). Both local and global simulations have been performed with and without net flux. In both cases prolific density wave excitation has been noted (e.g. Gardiner & Stone (2006) in the local case and Armitage (1998) in the global case). These may be significant for explaining phenomena such as quasi periodic oscillations and more recently it has been suggested that the stochastic gravitational forces derived from such density variations may play an important role in driving the migration of low mass protoplanets (Nel-

son & Papaloizou 2004; Nelson 2005). Therefore it is important to gain an understanding of the processes leading to the excitation of these waves, how generic the phenomenon is, and how the wave amplitudes scale with physical parameters.

It is the purpose of this paper together with a following paper (Heinemann & Papaloizou 2008) (paper II) to investigate this phenomenon in detail. In this paper we develop a WKBJ theory for the excitation of these density waves which we hereafter refer to as inertial-acoustic (IA) waves. The object will be to describe the excitation process and calculate excited wave amplitudes and associated angular momentum transport. In paper II we perform numerical simulations which we use to study the wave excitation process and compare it in detail to the predictions of the WKBJ theory.

The plan of this paper is as follows: In section 2 we describe the shearing box model, giving the basic equations and defining the background shear flow in which the hydromagnetic turbulence responsible for the IA wave excitation, is generated. In section 3 we derive equations de-

scribing the excitation of IA waves. These take the form of linear wave equations with both linear and non-linear source terms that are determined by the turbulence. The situation is similar to the theory of sound generation by turbulence due to Lighthill (1952). Here, however, effects due to rotation, shear and magnetic fields have to be considered. We focus on waves that are nearly independent of the vertical coordinate which have been found to dominate in simulations carried out in paper II and which can be dealt with using a vertical averaging procedure. We go on to formulate the law of conservation of the wave action for this type of non dissipative IA waves, as the wave action, equivalent to the outward angular momentum flux, is used to estimate the angular momentum flux arising from the excited waves.

In section 4 we go on to develop a WKBJ theory for the wave excitation. A Fourier analysis is carried out enabling each azimuthal wave number  $k_y$  to be considered separately. The WKBJ theory applies to a shearing box for which the boundary conditions are the imposition of periodicity in shearing coordinates and involves a sequence of excitations uniformly spaced and localized in time, during which the wave swings from leading to trailing. The wave amplitude and wave action produced in a swing are calculated from a WKBJ formalism involving the evaluation of integrals along anti-Stokes lines.

In order to do these calculations, we assume weakly non linear conditions, under which the important source terms for exciting the IA waves are expected to be proportional to what we call the pseudo potential vorticity, which is equal to the potential vorticity in linear order but differs from it in the non linear regime. The above assumption is justified by the results of simulations carried out in paper II. The resulting theory has similarities to the theory of excitation of inertia-gravity waves in the earth's atmosphere and oceans excited by potential vorticity variations (see Vanneste & Yavneh 2004) which also requires a similar WKBJ approach.

We compare the results derived from asymptotic theory to results obtained by numerically integrating the ordinary differential equations describing the evolution of the appropriate Fourier amplitude. We find excellent agreement between these approaches. This agreement persists under all conditions of interest. This is in spite of the fact that asymptotic theory formally requires a parameter depending on the azimuthal wave number to be small. Finally we discuss our results in Section 5.

## 2 THE SHEARING BOX MODEL

### 2.1 Basic set up and equations

We consider a conducting gas in the shearing box approximation (Goldreich & Lynden-Bell 1965). A Cartesian coordinate system  $(x, y, z) \equiv \vec{x}$  with origin at the centre of the box is adopted. The system rotates with angular velocity  $\vec{\Omega} = \Omega \vec{e}_z$ , with  $\vec{e}_z$  being the unit vector in the  $z$ -direction. This coincides with the angular velocity of the centre of the box, taken to be in a circular orbit. In the Keplerian case this is about a central mass,  $M$ . The lengths of the sides of the box in the three coordinate directions are  $(L_x, L_y, L_z)$  and vertical stratification is neglected.

The basic equations are those of MHD for an isothermal

gas, i.e. the continuity equation

$$\frac{\partial \rho}{\partial t} + \nabla \cdot (\rho \vec{v}) = 0,$$

the momentum equation

$$\frac{\partial(\rho \vec{v})}{\partial t} = -c^2 \nabla \rho - 2\vec{\Omega} \times \rho \vec{v} - \rho \nabla \Phi + \nabla \cdot \mathbf{T}' + \nabla \cdot (2\rho \nu \mathbf{S})$$

and the induction equation

$$\frac{\partial \vec{B}}{\partial t} = \nabla \times (\vec{v} \times \vec{B}) + \eta \nabla^2 \vec{B},$$

where  $\rho$  is the density, the velocity is  $\vec{v} = (v_x, v_y, v_z)$ , the isothermal sound speed is  $c$ , the magnetic field is  $\vec{B} = (B_x, B_y, B_z)$ , the non-linear stress tensor  $\mathbf{T}'$  has components

$$T'_{ij} = B_i B_j - \delta_{ij} \vec{B}^2 / 2 - \rho v_i v_j,$$

and  $\mathbf{S}$  is the traceless rate-of-strain tensor whose components are given by

$$S_{ij} = \frac{1}{2} \left( \frac{\partial v_i}{\partial x_j} + \frac{\partial v_j}{\partial x_i} - \frac{2}{3} \delta_{ij} \nabla \cdot \vec{v} \right).$$

The kinematic viscosity is  $\nu$ , the resistivity is  $\eta$ , and the combined gravitational and centrifugal potential is given by

$$\Phi = -q\Omega^2 x^2,$$

where for a Keplerian flow the constant  $q = 3/2$ .

The isothermal MHD equations admit the definition of a characteristic length scale  $H = c/\Omega$ , which we will refer to as the putative disc scale height even though we have neglected vertical stratification.

### 2.2 Equations for deviations from the steady state and boundary conditions

The background state is taken to have uniform density  $\rho_0$ , zero magnetic field and a linear shear corresponding to the velocity

$$\vec{v}_0 = -q\Omega x \vec{e}_y.$$

As we are interested in wave propagation we work in terms of velocity deviations from the background shear,  $\vec{u} = \vec{v} - \vec{v}_0$ , which we use to define the linear momentum density per unit volume  $\vec{p} = \rho \vec{u}$ . In terms of  $\rho$  and  $\vec{p}$  the governing equations now read

$$\mathcal{D}\rho + \nabla \cdot \vec{p} = 0, \quad (1)$$

$$\mathcal{D}\vec{p} = -c^2 \nabla \rho - 2\vec{\Omega} \times \vec{p} + q\Omega p_x \vec{e}_y + \nabla \cdot \mathbf{T} + \nabla \cdot (2\rho \nu \mathbf{S}), \quad (2)$$

$$\mathcal{D}\vec{B} = \nabla \times (\vec{u} \times \vec{B}) - q\Omega B_x \vec{e}_y + \eta \nabla^2 \vec{B}, \quad (3)$$

where the differential operator

$$\mathcal{D} = \frac{\partial}{\partial t} - q\Omega x \frac{\partial}{\partial y} \quad (4)$$

accounts for advection by the linear shear. Note that here, the non-linear stress tensor

$$T_{ij} = B_i B_j - \delta_{ij} \vec{B}^2 / 2 - \rho u_i u_j \quad (5)$$

only contains products of deviations from the background state.

We consider equations (1) to (3) to be subject to periodic boundary conditions in ‘Lagrangian’ (or ‘sheared’) coordinates given by

$$x' = x, \quad y' = y + q\Omega t x, \quad z' = z, \quad \text{and} \quad t' = t, \quad (6)$$

transformation to which removes the explicit  $x$ -dependence contained in (4) – albeit at the expense of an explicit time dependence<sup>1</sup>. Re-expressed in ‘Eulerian’ coordinates  $(x, y, z, t)$  the radial boundary condition for any fluid variable  $f$  then reads

$$f(x + L_x, y - q\Omega t L_x, z, t) = f(x, y, z, t)$$

while the azimuthal and vertical boundary conditions are simply

$$f(x, y + L_y, z, t) = f(x, y, z, t)$$

and

$$f(x, y, z + L_z, t) = f(x, y, z, t),$$

respectively.

### 3 WAVE EQUATIONS WITH SOURCES

In order to proceed we develop equations for the deviation of the state variables from their background state in order to obtain wave equations with sources. These can then be used to study the excitation of inertial-acoustic waves explicitly, much as in the spirit of Lighthill’s theory of the excitation of sound waves by turbulence (Lighthill 1952). It is known that inertial-acoustic waves can propagate in a strictly isothermal box with no dependence on the vertical coordinate (see Fromang & Papaloizou 2007) and we have found that such waves are the ones predominantly excited in our simulations presented in paper II. It is possible to vertically average equations (1) and (2), which then become equations for the vertical averages of the state variables such as  $\bar{p}$  and  $\rho$ , in order to describe such waves. When periodic boundary conditions in  $z$  are adopted this can be done without approximation and it is equivalent to adopting  $k_z = 0$  when Fourier transforms are considered. Proceeding in this way, we denote the vertical average of a quantity  $f$  by use of angle brackets as  $\langle f \rangle_z$ .

To further simplify the analysis we consider the inviscid limit of the shearing box equations, which then become

$$\mathcal{D} \langle \rho \rangle_z + \partial_x \langle p_x \rangle_z + \partial_y \langle p_y \rangle_z = 0 \quad (8a)$$

$$\mathcal{D} \langle p_x \rangle_z + c^2 \partial_x \langle \rho \rangle_z - 2\Omega \langle p_y \rangle_z = \langle \mathfrak{N}_x \rangle_z \quad (8b)$$

$$\mathcal{D} \langle p_y \rangle_z + c^2 \partial_y \langle \rho \rangle_z - (q - 2)\Omega \langle p_x \rangle_z = \langle \mathfrak{N}_y \rangle_z \quad (8c)$$

where we introduced the short-hand  $\vec{\mathfrak{N}} = \nabla \cdot \mathbf{T}$ . At this point we note that in the zero net flux case considered here, the magnetic field enters the momentum equation only through the non-linear stress tensor (5) so that it will not affect the description of linear IA waves.

Acting on (8c) with  $\mathcal{D}$  and rearranging terms yields

$$(\mathcal{D}^2 - c^2 \nabla^2 + \kappa^2) \langle p_y \rangle_z = -c^2 \partial_x \langle \zeta \rangle_z + (q - 2)\Omega \langle \mathfrak{N}_x \rangle_z + \mathcal{D} \langle \mathfrak{N}_y \rangle_z \quad (9)$$

<sup>1</sup> Without loss of generality we have assumed that the two coordinate systems coincide at  $t = 0$ .

where  $\kappa^2 = 2(2 - q)\Omega^2$  is the square of the epicyclic frequency and

$$\zeta = \partial_x p_y - \partial_y p_x + (q - 2)\Omega \rho$$

we shall call the pseudo potential vorticity (PPV). To linear order, the variation of PPV is equal to the variation of the so-called potential vorticity (PV),

$$Q = \frac{\partial_x u_y - \partial_y u_x + (2 - q)\Omega}{\rho},$$

(see Johnson & Gammie 2005). Written out explicitly, we have

$$\zeta - \zeta_0 = \rho_0^2 (Q - Q_0) + \text{non-linear terms},$$

where

$$\zeta_0 = (q - 2)\Omega \rho_0 \quad \text{and} \quad Q_0 = \frac{(2 - q)\Omega}{\rho_0}$$

are the steady state background values of PPV and PV, respectively. For disturbances with  $k_z = 0$  and given a barotropic equation of state, PV is an exactly conserved quantity whereas PPV varies due to non-linear stresses,

$$\mathcal{D} \langle \zeta \rangle_z = \partial_x \langle \mathfrak{N}_y \rangle_z - \partial_y \langle \mathfrak{N}_x \rangle_z. \quad (10)$$

We can form wave equations similar to (9) for  $\rho$  and  $p_x$ . Letting  $\mathcal{D}$  act on (8a) and (8b) yields

$$(\mathcal{D}^2 - c^2 \nabla^2 + \kappa^2) \langle \rho \rangle_z + 2q\Omega \partial_y \langle p_x \rangle_z = -2\Omega \langle \zeta \rangle_z - \partial_x \langle \mathfrak{N}_x \rangle_z - \partial_y \langle \mathfrak{N}_y \rangle_z \quad (11a)$$

and

$$(\mathcal{D}^2 - c^2 \nabla^2 + \kappa^2) \langle p_x \rangle_z + 2q\Omega c^2 \partial_y \langle \rho \rangle_z = c^2 \partial_y \langle \zeta \rangle_z + 2\Omega \langle \mathfrak{N}_y \rangle_z + \mathcal{D} \langle \mathfrak{N}_x \rangle_z. \quad (11b)$$

#### 3.1 Decomposition into shearing waves

In the periodic shearing sheet we may expand all fluid variables in a series of plane wave solutions

$$\exp(i k'_x x' + i k'_y y')$$

in the Lagrangian coordinate frame (6). Here, the radial and azimuthal wave numbers

$$k'_x = \frac{2\pi n_x}{L_x} \quad \text{and} \quad k'_y = \frac{2\pi n_y}{L_y} \quad \text{with} \quad n_x, n_y \in \mathbb{Z}.$$

In terms of Eulerian coordinates, the plane wave expansion for any (vertically averaged) fluid variable  $\langle f \rangle_z$  reads

$$\langle f \rangle_z(x, y, t) = \sum_{n_x, n_y} \hat{f}(t) \exp[i k_x(t) x + i k_y y]$$

with a time dependent radial wave number

$$k_x(t) = k'_x + q\Omega t k'_y. \quad (12)$$

and constant azimuthal wave number  $k_y = k'_y$ .

When viewed from the Eulerian coordinate frame, the radial wave number of non-axisymmetric disturbances (for which  $k_y \neq 0$ ) changes linearly in time due to advection by the linear shear, leading to the notion of sheared disturbances as originally discussed by Kelvin (Thomson 1887). In the shearing sheet, non-axisymmetric plane waves are therefore often referred to as shearing waves.

It is customary to classify shearing waves according to whether they are leading, i.e.  $k_x(t)/k_y < 0$ , or trailing, i.e.  $k_x(t)/k_y > 0$ . Because the time dependence of the radial wave number (12) is such that  $k_x(t)/k_y$  always increases monotonically provided that  $q\Omega > 0$ , every leading wave will eventually become trailing as time progresses. The change from leading to trailing is referred to as ‘swing’ and occurs when  $k_x(t) = 0$ . Different shearing waves swing from leading to trailing at different times so that the excitation process consists of a series of swings that are separated, for a given  $k_y$ , by a fixed time interval

$$\delta t_s = \frac{T_{\text{orb}}}{qk_y L_x}, \quad (13)$$

where  $T_{\text{orb}} = 2\pi/\Omega$  is the orbital period.

We note that because we are dealing with the Fourier transforms of real quantities, each Fourier coefficient becomes equal to its complex conjugate under reflection of the wave number such that  $\vec{k} \rightarrow -\vec{k}$ . This means that we may without loss of generality consider only  $k_y > 0$ , and then multiply by a factor of two after taking the real part of the transforms to obtain physical quantities, which then accounts for  $k_y < 0$ . Thus from now on we consider only  $k_y > 0$ .

It is now straightforward to write down the IA wave equations (9) and (11) in Fourier space. Substituting

$$\mathcal{D} \rightarrow d/dt, \quad \partial_x \rightarrow ik_x(t), \quad \text{and} \quad \partial_y \rightarrow ik_y$$

we readily obtain

$$\begin{aligned} \frac{d^2 \hat{\rho}}{dt^2} + [\vec{k}^2(t)c^2 + \kappa^2] \hat{\rho} + 2q\Omega ik_y \hat{p}_x = \\ - 2\Omega \hat{\zeta} - ik_x(t) \hat{\mathfrak{N}}_x - ik_y \hat{\mathfrak{N}}_y, \end{aligned}$$

$$\begin{aligned} \frac{d^2 \hat{p}_x}{dt^2} + [\vec{k}^2(t)c^2 + \kappa^2] \hat{p}_x + 2q\Omega c^2 ik_y \hat{\rho} = \\ c^2 ik_y \hat{\zeta} + 2\Omega \hat{\mathfrak{N}}_y + \frac{d\hat{\mathfrak{N}}_x}{dt}, \end{aligned}$$

and

$$\frac{d^2 \hat{p}_y}{dt^2} + [\vec{k}^2(t)c^2 + \kappa^2] \hat{p}_y = -c^2 ik_x \hat{\zeta} + (q-2)\Omega \hat{\mathfrak{N}}_x + \frac{d\hat{\mathfrak{N}}_y}{dt}.$$

### 3.2 Wave action

Conservation of angular momentum for linear waves in the shearing box follows from invariance of the system under translations along the azimuthal or  $y$ -direction. Here we note that this actually yields a momentum flux that can be converted into an angular momentum flux by multiplying by the radius of the centre of the box. As the latter quantity does not play any role in the box dynamics we can conveniently set it to be unity making the momentum and angular momentum fluxes equivalent. We introduce the Lagrangian displacement which we define through

$$\mathcal{D}\vec{\xi} = \vec{p}/\rho_0 - q\Omega \xi_x \vec{e}_y \quad (15)$$

In terms of  $\vec{\xi}$ , the density deviations from the background state are given by

$$\delta\rho/\rho_0 + \nabla \cdot \vec{\xi} = 0$$

and the linearised equations of motion become

$$\mathcal{D}^2 \vec{\xi} = c^2 \nabla \nabla \cdot \vec{\xi} - 2\vec{\Omega} \times \mathcal{D}\vec{\xi} + 2q\Omega^2 \xi_x \vec{e}_x.$$

These also follow by varying the action  $\int \mathcal{L} d^3\vec{x} dt$  where the Lagrangian density

$$\mathcal{L} = \frac{\rho_0}{2} [\mathcal{D}\vec{\xi} \cdot \mathcal{D}\vec{\xi} - c^2 (\nabla \cdot \vec{\xi})^2 + 2(\vec{\Omega} \times \vec{\xi}) \cdot \mathcal{D}\vec{\xi} + 2q\Omega^2 \xi_x^2].$$

Requiring invariance to translations in the  $y$  direction through the condition  $d\mathcal{L}/dy = 0$  yields the conservation law,

$$\mathcal{D}A + \nabla \cdot \vec{F} = 0 \quad (16)$$

where the angular momentum density

$$A = -\rho_0 (\mathcal{D}\vec{\xi} + \vec{\Omega} \times \vec{\xi}) \cdot \partial_y \vec{\xi} \quad (17)$$

and the associated flux

$$\vec{F} = -c^2 \delta\rho \partial_y \vec{\xi} - \mathcal{L} \vec{e}_y \quad (18)$$

This is an expected consequence of Noether’s theorem. However, note the negative sign in equations (17) and (18) (see also Goodman & Ryu 1992). We see that axisymmetric waves with  $\partial_y = 0$  transport no angular momentum. Note that the angular momentum conservation (16) law may be averaged over  $y$  and  $z$  to read

$$\partial_t \langle A \rangle_{yz} + \partial_x \langle F_x \rangle_{yz} = 0.$$

This definition of angular momentum flux is, at times, inconvenient to work with because it involves the Lagrangian displacement  $\vec{\xi}$ . We can derive a related wave action where the radial flux only depends on mass density and momentum density as follows. From (8c) and (15) we have to linear order

$$\xi_x = \frac{p_y + c^2 \partial_y W}{(q-2)\Omega\rho_0}, \quad \text{where } \mathcal{D}W = \delta\rho. \quad (19)$$

Inserting (19) into (18) yields after some straightforward algebra

$$\begin{aligned} F_x = -\frac{c^2}{(q-2)\Omega\rho_0} \\ \left\{ \delta\rho \partial_y p_y + \partial_y \left( c^2 \delta\rho \partial_y W \right) - \mathcal{D} \left[ \frac{c^2}{2} \left( \partial_y W \right)^2 \right] \right\}. \end{aligned}$$

The second and the third term in curly brackets can be absorbed in the  $y$ -component of the angular momentum flux and in the angular momentum density, respectively, giving rise to a new wave action conservation law,

$$\mathcal{D}A' + \nabla \cdot \vec{F}' = 0,$$

where the modified radial angular momentum flux

$$F'_x = -\frac{c^2 \delta\rho \partial_y p_y}{(q-2)\Omega\rho_0}.$$

has the desired property that it does not involve the Lagrangian displacement. Furthermore, this new flux is equal to the radial component of the angular momentum flux (18) after averaging over  $y$ ,  $z$ , and  $t$ . But it should be noted that it in order to establish this equality it has been assumed that no external forces act in the domain.

We will define a suitable temporal averaging procedure further below in Section 4.11. At this point we note that when evaluated for a single pair of (complex conjugate) shearing waves, and averaged over both  $y$  and  $z$ , the two

equivalent expressions for the radial angular momentum flux become

$$\langle F_x \rangle_{yz} = -2k_y c^2 \text{Im}(\hat{\xi}_x^* \hat{\rho}) \quad (20)$$

and

$$\langle F'_x \rangle_{yz} = \frac{2k_y c^2}{(2-q)\Omega\rho_0} \text{Im}(\hat{p}_y^* \hat{\rho}). \quad (21)$$

Here, without loss of generality, we have adopted  $k_y > 0$  as described in Section 3.1.

#### 4 WKBJ THEORY OF WAVE EXCITATION

In this section we derive a WKBJ theory of the wave excitation that occurs during a swing cycle and derive an expression for the wave action produced. We go on to compare this theory in detail with the results of numerical integrations of the ordinary differential equations governing the time dependent evolution of the Fourier transforms of the wave amplitudes for a simple model system. Good agreement is obtained. In paper II we compare results obtained from the WKBJ theory with those obtained from MRI simulations.

##### 4.1 The nature of the source terms

We first need to establish which of the source terms on the right hand sides of (14) are primarily responsible for wave excitation. Inspection of these equations shows that the source terms are of two kinds. The first kind is proportional to the transform of PPV and the second kind is proportional to the non-linear stress tensor. Only terms of the first kind remain in the linear regime. Thus under conditions of weak non-linearity, we would expect them to dominate. An analysis of the relative contributions found in direct simulations given in paper II shows that the contribution of the pseudo potential vorticity related terms is the more important by an order of magnitude confirming the above idea. It is also shown that the strength of the wave excitation phenomenon for a swinging wave is directly correlated with the amplitude of the pseudo potential vorticity transform at the time of the transition from leading to trailing. Here we reiterate that although the generation of PPV itself is driven by the non-linear stresses, see (10), the linear source terms involving PPV survive at linear order if there is a build up over time under conditions of weak non-linearity.

Following on from the above discussion, from now on we retain only source terms that depend on the pseudo potential vorticity. These are proportional to  $\hat{\zeta}$  which we recall is a Fourier amplitude which is given by

$$\hat{\zeta}(t) = \frac{1}{L_x L_y} \int_0^{L_x} \int_0^{L_y} \langle \zeta \rangle_z(x, y, t) \exp[ik_x(t)x + ik_y y] dx dy$$

From the above expression we note that if  $\langle \zeta \rangle_z(x, y, t)$  is an ultimately smooth function, the Riemann Lebesgue lemma allows us to infer that the source is negligible as  $t \rightarrow \pm\infty$  and so is expected to peak around  $t = 0$  when the wave swings from leading to trailing. Thus the wave amplitude excitation process should also be localized around this time. At this point we recall that in a shearing box the wave excitation process for a fixed  $k_y$  appears as a succession of swings, which as seen from (12) are separated by the time

interval (13). For the longest possible wave length in the  $y$  direction given by the box size this is  $L_y/(2\pi q L_x)$  orbital periods. This is independent of the box size as long as the aspect ratio is fixed. Although this time interval formally decreases as  $L_x$  increases, because of the periodic symmetry associated with the shearing box, we expect results to be independent of  $L_x$  once this is larger than the radial correlation length associated with the turbulence, expected to be  $\sim H$ . Accordingly we might expect the phenomenon to take a similar form in global simulations (e.g. Nelson 2005).

##### 4.2 Reduction to three uncoupled second order oscillator equations

As motivated above we will now neglect any non-linearities in the problem. After dropping the non-linear source terms appearing in the IA wave equations (9) and (11) the evolution of  $\rho$ ,  $p_x$ , and  $p_y$  in Fourier space is governed by

$$\frac{d^2 \hat{\rho}}{dt^2} + (\tilde{k}^2 c^2 + \kappa^2) \hat{\rho} + 2q\Omega i k_y \hat{p}_x = -2\Omega \hat{\zeta}, \quad (22a)$$

$$\frac{d^2 \hat{p}_x}{dt^2} + (\tilde{k}^2 c^2 + \kappa^2) \hat{p}_x + 2q\Omega c^2 i k_y \hat{\rho} = c^2 i k_y \hat{\zeta}, \quad (22b)$$

and

$$\frac{d^2 \hat{p}_y}{dt^2} + (\tilde{k}^2 c^2 + \kappa^2) \hat{p}_y = -c^2 i k_x \hat{\zeta}. \quad (23)$$

We note that in the absence of non-linearities the pseudo potential vorticity,

$$\hat{\zeta} = i k_x \hat{p}_y - i k_y \hat{p}_x + (q-2)\Omega \hat{\rho}, \quad (24)$$

is conserved exactly, i.e.

$$\frac{d\hat{\zeta}}{dt} = 0. \quad (25)$$

The wave equation for  $\hat{p}_y$ , given by (23), therefore decouples from those for  $\hat{\rho}$  and  $\hat{p}_x$ , given by (22). The latter two equations may be decoupled from each other as well by introducing the pair

$$\hat{p}_{\pm} = \hat{p}_x \pm \hat{\rho} c, \quad (26)$$

for which the linearised wave equations read

$$\frac{d^2 \hat{p}_{\pm}}{dt^2} + (\tilde{k}^2 c^2 + \kappa^2 \pm 2q\Omega i k_y c) \hat{p}_{\pm} = c(i k_y c \mp 2\Omega) \hat{\zeta}. \quad (27)$$

We can simplify (23) and (27) further by introducing the dimensionless time variable

$$\tau = \frac{k_x c}{\sqrt{k_y^2 c^2 + \kappa^2}} \quad (28)$$

and the dimensionless parameter

$$\epsilon = \frac{q\Omega k_y c}{k_y^2 c^2 + \kappa^2} \quad (29)$$

in terms of which we have

$$\epsilon^2 \frac{d^2 \hat{p}_y}{d\tau^2} + (\tau^2 + 1) \hat{p}_y = -c \left( \frac{i k_x c}{k_y^2 c^2 + \kappa^2} \right) \hat{\zeta} \quad (30a)$$

and

$$\epsilon^2 \frac{d^2 \hat{p}_{\pm}}{d\tau^2} + (\tau^2 + 1 \pm 2i\epsilon) \hat{p}_{\pm} = c \left( \frac{i k_y c \mp 2\Omega}{k_y^2 c^2 + \kappa^2} \right) \hat{\zeta}. \quad (30b)$$

The form of these equations suggests an asymptotic expansion in  $\epsilon$ . Formally, such an expansion is valid if  $\epsilon \ll 1$ . From (29) we can see that this will be the case both in the high and the low azimuthal wave number limit given by  $k_y c \gg \kappa$  and  $k_y c \ll \kappa$ , respectively.

In the following, we will derive asymptotic solutions to (30) based on the smallness of  $\epsilon$ . However, we will demonstrate that these approximative solutions show excellent agreement with the exact solution obtained from direct numerical integration even in the worst possible case of  $k_y c = \kappa$  for which  $\epsilon$  attains its maximum value,  $\epsilon^{\max} = q\Omega/2\kappa$ .

### 4.3 Slowly varying solutions

We consider equations (30) for large  $|\tau|$ , i.e. in the high radial wave number limit. In this limit the second time derivatives are significant only for solutions that vary rapidly in  $\tau$ . Such solutions are expected when sources are absent and correspond to high frequency oscillations. This suggests that they can be dropped for solutions that vary slowly with  $\tau$ . As a first approximation, we drop the double time derivative in (30) to obtain

$$\bar{p}_y = -c \left( \frac{ik_x c}{\vec{k}^2 c^2 + \kappa^2} \right) \hat{\zeta} \quad (31a)$$

and

$$\bar{p}_{\pm} = c \left( \frac{ik_y c \mp 2\Omega}{\vec{k}^2 c^2 + \kappa^2 \pm 2q\Omega ik_y c} \right) \hat{\zeta}, \quad (31b)$$

where we have used (28) and (29). These approximative solutions to inhomogeneous problem are the leading order terms of an asymptotic series expansion in ascending powers of  $\epsilon$ . The series diverges near the time of the swing from leading to trailing, i.e. near  $\tau = 0$ , when the double time derivative in (30) becomes significant and oscillatory solutions to the homogeneous equation must be taken into account.

The occurrence of such oscillatory solutions may easily be demonstrated by direct numerical integration of (30), which is just a set of linear ordinary differential equations. We start the integration in the far leading phase, i.e. at  $\tau = \tau_0$  with  $\tau_0$  large and negative. In this limit the balanced solutions (31) hold and may be used as initial conditions. We note that in doing so we have to be careful not to violate PPV conservation which we know to be exact in linear theory, see (25). This problem arises on account of the additional time derivative taken to obtain (9) and (11) from (8).

Formally, the balanced solutions (31) are reconcilable with PPV conservation only in the limit  $\tau \rightarrow \pm\infty$ . We thus introduce an error if we use these solutions as initial conditions at some finite  $\tau_0$  and we have to make sure that  $\tau_0$  is sufficiently large so that this error is small. In order to be able to quantify this error during the course of the integration, we express the PPV  $\hat{\zeta}$  in terms of  $r\hat{\rho}$  and  $\hat{p}_x$ , see (24) together with (26), and solve (30) as a system of three coupled ordinary differential equations. PPV conservation is not guaranteed in this case, but we find empirically that the numerical integration conserves PPV arbitrarily well depending on how large  $\tau_0$  (and thus the error introduced by using the balanced solutions as initial conditions) is.

Bearing these general remarks in mind, we now discuss

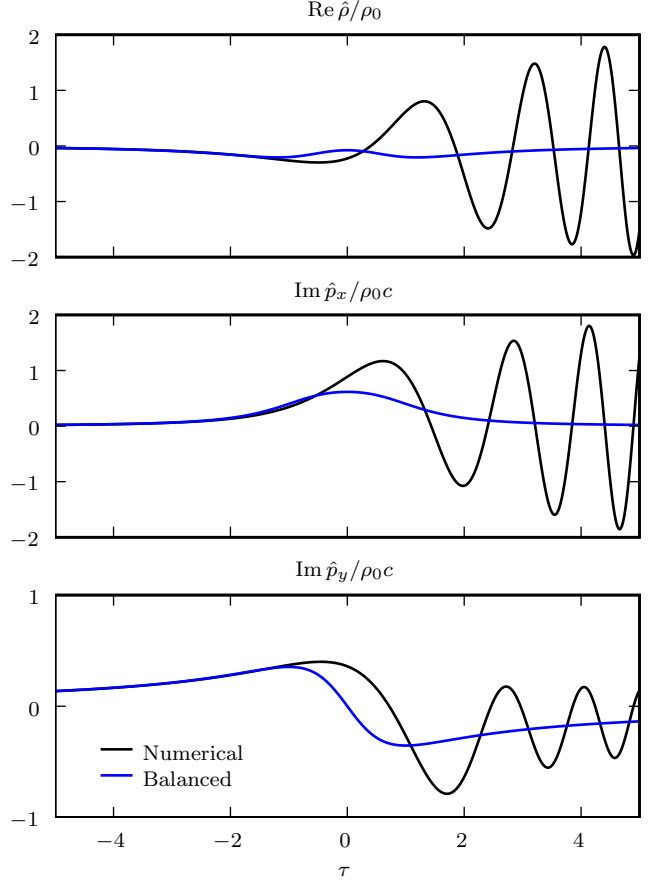


**Figure 1.** Comparison between the numerical solution (black) to the simplified wave equations (30) with the corresponding balanced solutions (blue). Here we have used (26) to compute  $\hat{\rho}$  and  $\hat{p}_x$  from  $\hat{p}_{\pm}$ . The parameters in this example are  $q = 3/2$ ,  $\epsilon = 3/4$ , and  $\hat{\zeta} = \Omega\rho_0$ . In the lowermost panel,  $\hat{p}_y$  was obtained from (58), while in the panel immediately above it was obtained from (52).

a specific numerical solution to (30). For this purpose we consider Keplerian shear, i.e.  $q = 3/2$ . Because we would like to determine empirically how well asymptotic theory works when we are far away from the asymptotic limit  $\epsilon \ll 1$  we take the worst possible case, i.e. a shearing wave with  $k_y = \kappa/c = 1/H$  so that  $\epsilon = q\Omega/2\kappa = 3/4$ . For the determination of the initial conditions from the balanced solutions we assume, without loss of generality, that  $\hat{\zeta} = \Omega\rho_0$  in (31).

We start the integration at  $\tau = -100$ .<sup>2</sup> The evolution of the Fourier amplitudes near the swing from leading to trailing as a function of the radial wave number is shown in Fig. 1. Before the swing from leading to trailing the numerical solution closely follows the balanced solution up until  $\tau \approx 0$  where a sudden transition to oscillatory behaviour occurs. In the trailing phase, the numerical solution oscillates with a relatively large but rather slowly evolving amplitude around the balanced solution. Such oscillatory be-

<sup>2</sup> At this point the relative error as far as PPV conservation is concerned is  $\sim 10^{-8}$ . We find that the relative error never exceeds  $10^{-6}$  during the entire course of the integration from  $\tau = -100$  to  $\tau = 10$ .

haviour cannot be captured by a perturbation series expansion. In order to describe it we have to resort to singular perturbation theory to be discussed in the next section.

#### 4.4 WKBJ solution of the generic oscillator equation

To study the excitation of a general Fourier mode we seek a solution to the forced harmonic oscillator equation of the general type

$$\epsilon^2 \frac{d^2 y(\tau)}{d\tau^2} + (\tau^2 + a^2)y(\tau) = f(\tau) \quad (32)$$

with  $\epsilon \ll 1$  and where  $a$  is a complex number with

$$|a| \sim O(1) \quad \text{and} \quad |\text{ph } a| < \pi/4, \quad (33)$$

the latter being true for  $a = \sqrt{1 + 2i\epsilon}$  with  $0 \leq \epsilon < \infty$ .

Throughout the following analysis make  $w = z^{1/n}$  single-valued by taking the branch cut along the negative real axis and always take the principal branch, thus

$$\text{ph } w = \frac{\text{ph } z}{n}. \quad (34)$$

We note that equations (30a) and (30b) are special cases of the above general form. We further also assume that  $f(\tau)$  is a slowly varying function such that  $\Delta f \sim O(1)$  for  $\Delta\tau \sim O(1)$  as  $\epsilon \rightarrow 0$ . Physically this means that the pseudo potential vorticity transform should vary at a slow rate compared to the wave oscillation frequency at around the time of the swing. This is expected under conditions of weak nonlinearity as discussed in section 4.1 and simulation results presented in paper II indicate that this is indeed the case.

#### 4.5 Outer and balanced solutions

A solution of equation (32) in ascending powers of  $\epsilon^2$  is readily found from regular perturbation theory, and yields to lowest order

$$y(\tau) = \frac{f(\tau)}{\tau^2 + a^2} + O(\epsilon^2), \quad (35)$$

which is, given (33), well defined on the entire real axis. However, this series, giving rise to what is described as the balanced solution, is only asymptotic, no matter to what order in  $\epsilon^2$  we go, the series will fail to represent rapidly changing oscillatory contributions to  $y(\tau)$  for which the double derivative term in (32) is significant. These vanish more rapidly than any power of  $\epsilon$  as  $\epsilon \rightarrow 0$ .

In order to obtain these contributions, that are in fact associated with the excited IA waves, we have to resort to singular perturbation theory. We thus seek a solution of the asymptotic form

$$y(\tau) \approx \frac{f(\tau)}{\tau^2 + a^2}, \quad \tau \rightarrow -\infty \quad (36)$$

$$y(\tau) \approx \frac{f(\tau)}{\tau^2 + a^2} + \frac{A_+ e^{-i\Phi(\tau)/\epsilon}}{(\tau^2 + a^2)^{1/4}} + \frac{A_- e^{+i\Phi(\tau)/\epsilon}}{(\tau^2 + a^2)^{1/4}}, \quad \tau \rightarrow +\infty \quad (37)$$

which is the sum of the leading order solution to the inhomogeneous problem obtained from regular perturbation

theory, and a standard WKBJ solution to the homogeneous problem. Here the WKBJ phase is given by

$$\begin{aligned} \Phi(\tau) &= \int_0^\tau \sqrt{\sigma^2 + a^2} d\sigma \\ &= \frac{1}{2} \left[ \tau \sqrt{\tau^2 + a^2} + a^2 \ln \left( \frac{\tau + \sqrt{\tau^2 + a^2}}{\sqrt{a^2}} \right) \right]. \end{aligned} \quad (38)$$

The associated WKBJ solution is identified with an excited wave.

#### 4.6 Matching on anti-Stokes lines

In order to determine the WKBJ (or wave) amplitudes  $A_+$  and  $A_-$ , we analytically continue the WKBJ solution (37) into the complex  $\tau$ -plane and match it to inner solutions valid in the immediate vicinity of the two complex WKBJ turning points at  $\tau_* = \pm ia$ . Thus in this section the  $\pm$  alternative refers to the turning point with positive and negative imaginary part respectively rather than the  $\hat{p}_\pm$  alternative of the previous section. We find it convenient to match inner and outer solutions along the so-called anti-Stokes lines defined by

$$\text{Im } \Phi(\tau) = \text{Im } \Phi(\tau_*). \quad (39)$$

Because the imaginary part of the WKBJ phase is constant on these lines, one of the WKBJ exponentials in (37) is maximally sub-dominant to the other one and may thus be ignored.

From the first order Taylor expansion about a turning point we have

$$\tau^2 + a^2 \approx 2\tau_*(\tau - \tau_*) \quad (40)$$

and therefore from equation (38) we obtain

$$\Phi(\tau) \approx \Phi(\tau_*) + \frac{2\sqrt{2}}{3} \tau_*^{1/2} (\tau - \tau_*)^{3/2}$$

The condition (39) thus defines three anti-Stokes lines emanating from each turning point at angles given by

$$\text{ph}(\tau - \tau_*) = \left( \mp \frac{5\pi}{6}, \mp \frac{\pi}{6}, \pm \frac{\pi}{2} \right) - \frac{\text{ph } a}{3}$$

For consistency we match on the anti-Stokes lines originating from each turning point that asymptotically approach the real axis.

For  $\text{Re } \tau < \text{Re}(\pm ia)$  these are

$$\text{ph}(\tau - \tau_*) = \mp \frac{5\pi}{6} - \frac{\text{ph } a}{3} \quad (41)$$

and for  $\text{Re } \tau > \text{Re}(\pm ia)$

$$\text{ph}(\tau - \tau_*) = \mp \frac{\pi}{6} - \frac{\text{ph } a}{3} \quad (42)$$

Note that with the definition of the square root obtained from (34), the WKBJ solution (37) has branch cuts that leave the turning points at an angle

$$\text{ph}(\tau - \tau_*) = \pm \frac{\pi}{2} - \text{ph } a$$

so we can always match along the anti-Stokes lines specified above without crossing branch cuts. This is illustrated in Fig. 2.

On an anti-Stokes line one of the two WKBJ exponentials in (37) will be maximally sub-dominant to the other

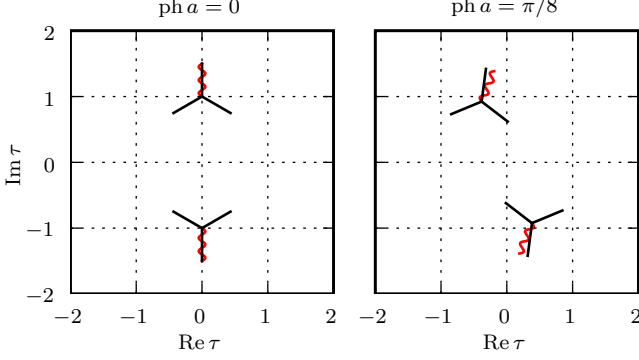


**Figure 2.** Anti-Stokes lines (solid black) emanating from the two turning points for  $\text{ph } a = 0$  (left panel) and  $\text{ph } a = \pi/8$  (right panel). The curly red curves indicate branch cuts.

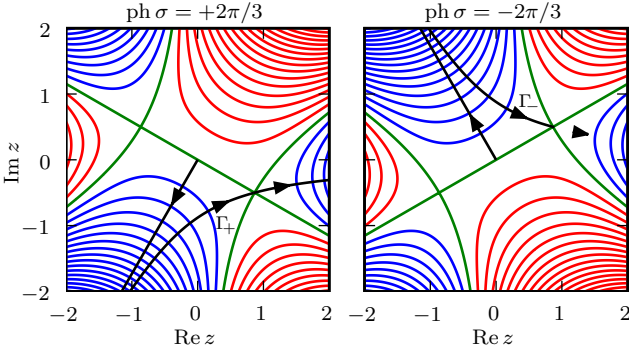


**Figure 3.** Integration contours for the Airy-integral (47) in the  $z$  plane. In each case the contour is deformed from the positive real axis to the two black lines shown. These contours which extend to infinity, correspond to the situation where we are on the anti-Stokes lines that radiate away from the turning points towards the positive real axis on which  $\text{ph } \sigma = 2\pi/3$  at the upper turning point (left panel) and  $\text{ph } \sigma = -2\pi/3$  at the lower turning point (right panel).

in the limit  $\epsilon \rightarrow 0$ , depending on the sign of the imaginary part of the WKBJ phase at the turning point from which it emanates. At these we have

$$\Phi(\pm ia) = \pm ia^2 \pi/4$$

and thus when the conditions (33) are satisfied

$$\text{Im } \Phi(\pm ia) \gtrless 0.$$

This means in general that the maximally sub-dominant exponential has an amplitude smaller by a factor  $\propto \exp(-c_0/\epsilon)$ , where  $c_0$  is a constant of order unity when compared to the dominant one, which is very small for small  $\epsilon$ . Therefore it should be neglected. Dropping the maximally sub-dominant WKBJ exponential, in the vicinity of the turning points our WKBJ solution is to leading order in  $\tau \mp ia$

$$y(\tau) \sim \frac{f(\tau_*)}{2\tau_*(\tau - \tau_*)} + \frac{A_{\pm} e^{\pi a^2/4\epsilon}}{[2\tau_*(\tau - \tau_*)]^{1/4}} \exp \left[ \mp i\epsilon^{-1} \frac{2\sqrt{2}}{3} \tau_*^{1/2} (\tau - \tau_*)^{3/2} \right]$$

We see that matching on the anti-Stokes line emanating from the upper (lower) turning point will only enable us to determine the WKBJ amplitude  $A_+$  ( $A_-$ ). We will thus need to match on the anti-Stokes lines from both turning points in order to determine the full WKBJ solution.

#### 4.7 Inner solution

To obtain the inner solutions we consider the governing equation (32) in the vicinity of the turning points. Using the first order Taylor expansion around a turning point (40) this becomes

$$\epsilon^2 \frac{d^2 y(\tau)}{d\tau^2} + 2\tau_*(\tau - \tau_*)y(\tau) = f(\tau_*). \quad (43)$$

We now defined rescaled variables through

$$\sigma = e^{\pm 2\pi i/3} (2\tau_*)^{1/3} \epsilon^{-2/3} (\tau - \tau_*) \quad (44)$$

$$y(\tau) = e^{\pm 2\pi i/3} (2\tau_*)^{-2/3} \epsilon^{-2/3} f(\tau_*) \phi(\sigma) \quad (45)$$

The first of these indicates that the solutions we seek vary on a scale  $|\tau| \sim \epsilon^{2/3} \ll 1$ . This feature enables us to perform an asymptotic expansion valid for large  $|\sigma|$  and still remain in the vicinity of the turning points. In terms of the rescaled variables, equation (43) yields an inhomogeneous Airy-type equation

$$\frac{d^2 \phi(\sigma)}{d\sigma^2} + \sigma \phi(\sigma) = 1. \quad (46)$$

We remark that from equation (44) we deduce that

$$\text{ph } \sigma = 0 \quad \text{for} \quad \text{ph}(\tau - \tau_*) = \mp \frac{5\pi}{6} - \frac{\text{ph } a}{3}$$

which applies on the anti-Stokes lines given by (41) and

$$\text{ph } \sigma = \pm \frac{2\pi}{3} \quad \text{for} \quad \text{ph}(\tau - \tau_*) = \mp \frac{\pi}{6} - \frac{\text{ph } a}{3}$$

which applies on the anti-Stokes lines given by (42).

#### 4.8 Integral representation for the inner solutions

The solution to (46) can be written as an integral

$$\phi(\sigma) = \int_0^\infty e^{h(\sigma, z)} dz \quad \text{with} \quad h(\sigma, z) = -\sigma z - z^3/3 \quad (47)$$

We are interested in the large- $\sigma$  asymptotic behaviour of this solution, which is applicable on each of the anti-Stokes lines emanating from both turning points.

For the anti-Stokes lines corresponding to  $\text{ph } \sigma = 0$  we integrate along the positive real axis and get an end-point contribution via Watson's lemma

$$\phi(\sigma) \sim \frac{1}{\sigma} \quad (\sigma \rightarrow \infty, \text{ph } \sigma = 0)$$

or with (44) and (45)

$$y(\tau) \sim \frac{f(\tau_*)}{2\tau_*(\tau - \tau_*)}$$

which matches our outer solution (37) to the left of the turning points if there we set  $A_+ = A_- = 0$  consistent with the causality requirement of the lack of existence of excited waves for  $\tau \rightarrow -\infty$ .

For the anti-Stokes lines corresponding to  $\text{ph } \sigma = \pm 2\pi/3$  we deform the integration contour from



the positive real axis to a contour consisting of two separate line segments, writing

$$\int_0^\infty e^{h(\sigma, z)} dz = \int_0^\infty e^{\mp 2i\pi/3} e^{h(\sigma, z)} dz + \int_{\Gamma_\pm} e^{h(\sigma, z)} dz. \quad (48)$$

The first integral on the right hand side is evaluated along a straight line that goes from the origin to  $\infty e^{\mp 2i\pi/3}$ . Along this line,  $h(z)$  is purely real and negative, and we again get an end-point contribution via Watson's lemma,

$$\int_0^\infty e^{\mp 2i\pi/3} e^{h(z)} dz \sim \frac{1}{\sigma} \quad (\sigma \rightarrow \infty, \text{ph } \sigma = \pm 2\pi/3).$$

The curve  $\Gamma_\pm$  along which the second integral on the right hand side of (48) is taken goes from  $\infty e^{\mp 2i\pi/3}$  along a path of steepest descent through the saddle point  $z_s = \mp i\sigma^{1/2}$  and from there to  $\infty$ , see Fig. 3. In the limit  $\sigma \rightarrow \infty$ , most of the contribution to this integral will come from near the saddle point  $z_s$ , at which  $h(z_s) = \pm(2/3)i\sigma^{3/2}$  and so

$$\int_{\Gamma_\pm} e^{h(z)} dz \sim \frac{\pi^{1/2} e^{\pm(2/3)i\sigma^{3/2}}}{e^{\mp i\pi/4} \sigma^{1/4}} \quad (\sigma \rightarrow \infty, \text{ph } \sigma = \pm 2\pi/3).$$

We thus have

$$\phi(\sigma) \sim \frac{1}{\sigma} + \frac{\pi^{1/2} e^{\pm(2/3)i\sigma^{3/2}}}{e^{\mp i\pi/4} \sigma^{1/4}} \quad (\sigma \rightarrow \infty, \text{ph } \sigma = \pm 2\pi/3).$$

Using (44) and (45) we may reexpress the above solution in terms of  $y$  and  $\tau - \tau^*$  to obtain

$$y(\tau) \sim \frac{f(\tau_*)}{2\tau_*(\tau - \tau_*)} + \frac{e^{\pm 3\pi i/4} (\pi/\epsilon)^{1/2} f(\tau_*)}{(2\tau_*)^{3/4} (\tau - \tau_*)^{1/4}} \exp \left[ \mp i\epsilon^{-1} \frac{2\sqrt{2}}{3} \tau_*^{1/2} (\tau - \tau_*)^{3/2} \right]$$

We match this solution to our outer solution (37) in the neighbourhood of each turning point by equating the factors in front of the maximally dominant WKBJ exponentials. This then yields the amplitudes

$$A_\pm = \pm i f(\pm ia) \left( \frac{\pi}{2a\epsilon} \right)^{1/2} e^{-\pi a^2/4\epsilon}.$$

Using these, the full asymptotic solution takes the form

$$y(\tau) \approx \frac{f(\tau)}{\tau^2 + a^2} + \left( \frac{2\pi}{a\epsilon} \right)^{1/2} \frac{e^{-\pi a^2/4\epsilon}}{(\tau^2 + a^2)^{1/4}} \frac{1}{2i} \left[ f(-ia) e^{+i\Phi(\tau)/\epsilon} - f(ia) e^{-i\Phi(\tau)/\epsilon} \right]. \quad (49)$$

#### 4.9 Determination of the wavelike forms of $\hat{p}_y$ , $\hat{p}_\pm$ , $\hat{p}_x$ , and $\hat{p}$

We are now in a position to obtain explicit solutions for  $\hat{p}_y$  and  $\hat{p}_\pm$ . To bring the wave equation (30a) for  $\hat{p}_y$  into the form of the general oscillator equation (32) we set

$$a = 1 \quad \text{and} \quad f(\tau) = -\frac{i\tau\hat{\zeta}}{\sqrt{k_y^2 c^2 + \kappa^2}}.$$

To obtain the wavelike part of the solution, i.e. the component proportional to the WKBJ exponential, which we will

denote by a tilde,  $f(\tau)$  has to be evaluated at the complex turning point  $\tau_*$ . Because PPV is conserved in linear theory, i.e.  $\hat{\zeta} = \text{const}$ , this poses no difficulties and we immediately obtain

$$\tilde{p}_y = \frac{i\hat{\zeta}_s c}{\sqrt{k_y^2 c^2 + \kappa^2}} \sqrt{\frac{2\pi}{\epsilon}} \frac{e^{-\pi/4\epsilon}}{(\tau^2 + 1)^{1/4}} \cos[\Phi(\tau)/\epsilon], \quad (50)$$

where the WKBJ phase

$$\Phi(\tau) = \frac{1}{2} \left[ \tau \sqrt{\tau^2 + 1} + \ln \left( \tau + \sqrt{\tau^2 + 1} \right) \right]. \quad (51)$$

Using the definitions of  $\tau$  and  $\epsilon$ , respectively given by (28) and (29), we can rewrite the solution for  $\tilde{p}_y$  as

$$\tilde{p}_y = iH\hat{\zeta}_s \mathcal{A} \sqrt{\Omega/\omega} \cos \left( \int_0^t \omega dt' \right), \quad (52)$$

where the dimensionless amplitude

$$\mathcal{A} = \frac{\Omega^{1/2}}{(k_y^2 c^2 + \kappa^2)^{1/4}} \sqrt{\frac{2\pi}{\epsilon}} e^{-\pi/4\epsilon} \quad (53)$$

and we have defined the IA wave frequency

$$\omega = \sqrt{\vec{k}^2 c^2 + \kappa^2}.$$

This procedure is readily repeated to obtain explicit solutions for  $\hat{p}_\pm$ . In this case, comparison of the governing equation (30b) with (32) implies that we need to set

$$a = \sqrt{1 \pm 2i\epsilon} \quad \text{and} \quad f(\tau) = c \left( \frac{ik_y c \mp 2\Omega}{k_y^2 c^2 + \kappa^2} \right) \hat{\zeta}$$

The solutions for  $\tilde{p}_\pm$  determined from (49) are thus

$$\tilde{p}_\pm = i\hat{\zeta}_s c \left( \frac{2\Omega \mp ik_y c}{k_y^2 c^2 + \kappa^2} \right) \frac{1}{(1 \pm 2i\epsilon)^{1/4}} \sqrt{\frac{2\pi}{\epsilon}} \frac{e^{-\pi/4\epsilon}}{(\tau^2 + 1 \pm 2i\epsilon)^{1/4}} \sin(\Phi_\pm/\epsilon), \quad (54)$$

where the WKBJ phase

$$\Phi_\pm = \frac{1}{2} \left[ \tau \sqrt{\tau^2 + 1 \pm 2i\epsilon} + (1 \pm 2i\epsilon) \ln \left( \frac{\tau + \sqrt{\tau^2 + 1 \pm 2i\epsilon}}{\sqrt{1 \pm 2i\epsilon}} \right) \right].$$

It is important to note here that  $\Phi_\pm$  are not real with the consequence that quantities such as  $e^{i\Phi_\pm/\epsilon}$  have a power law as well as exponential dependence on  $\tau$  for large  $\tau$ .

Again, we rewrite (54) in more familiar terms using (28) and (29) to obtain

$$\tilde{p}_\pm = i\hat{\zeta}_s H \mathcal{A}_\pm \sqrt{\Omega/\omega_\pm} \sin \left( \int_0^t \omega_\pm dt' \right), \quad (55)$$

where this time the amplitude is given by

$$\mathcal{A}_\pm = \frac{\Omega^{1/2}}{(k_y^2 c^2 + \kappa^2 \pm 2q\Omega ik_y c)^{1/4}} \left( \frac{2\Omega \mp ik_y c}{\sqrt{k_y^2 c^2 + \kappa^2}} \right) \sqrt{\frac{2\pi}{\epsilon}} e^{-\pi/4\epsilon} \quad (56)$$

and the wave frequency is

$$\omega_\pm = \sqrt{\omega^2 \pm 2q\Omega ik_y c}.$$

Note that both the amplitude and the wave frequency are complex valued.

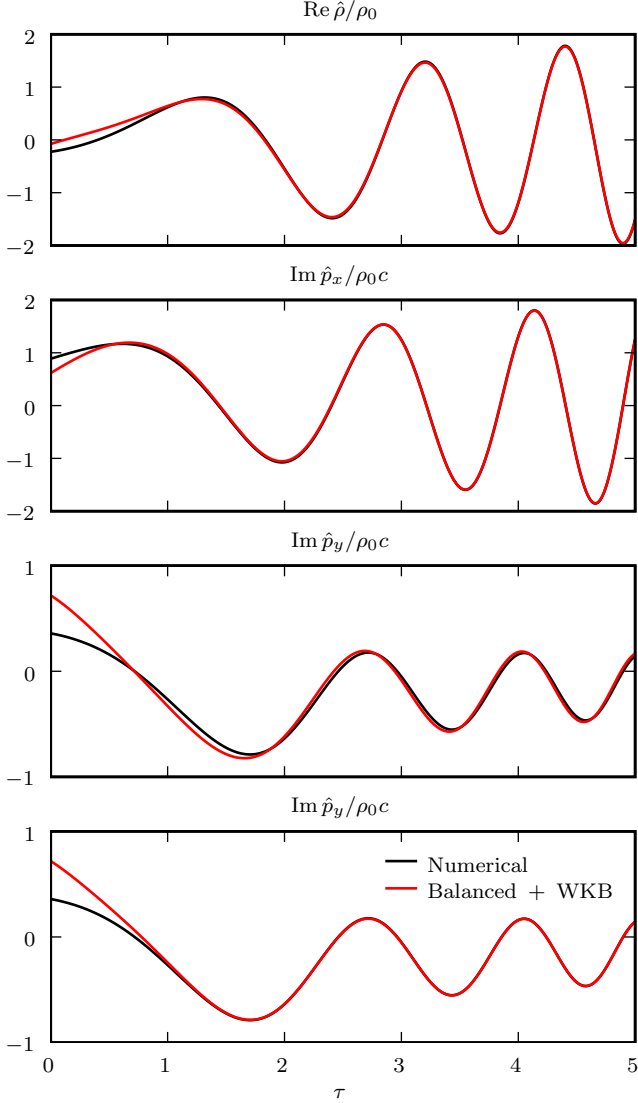


**Figure 4.** Comparison between the numerical solution (black) to the simplified wave equations (30) with the full asymptotic, i.e. balanced plus WKBJ, solution (red). The parameters are the same as in Fig. 1, i.e.  $q = 3/2$ ,  $\epsilon = 3/4$ , and  $\hat{\zeta} = \Omega\rho_0$ .

Recalling that  $\hat{p}_\pm = \hat{p}_x \pm \hat{p}_y$ , it is now a simple matter to determine the wavelike contributions to  $\hat{p}_x$  and  $\hat{p}_y$  in the forms

$$\tilde{\rho} = -\hat{\zeta}_s \Omega^{-1} \text{Im} \left[ \mathcal{A}_+ \sqrt{\Omega/\omega_+} \sin \left( \int_0^t \omega_+ dt' \right) \right] \quad (57a)$$

and

$$\tilde{p}_x = i\hat{\zeta}_s H \text{Re} \left[ \mathcal{A}_+ \sqrt{\Omega/\omega_+} \sin \left( \int_0^t \omega_+ dt' \right) \right] \quad (57b)$$

where we have used the fact that  $\mathcal{A}_+ = \mathcal{A}_-^*$  and  $\omega_+ = \omega_-^*$ .

We have seen in Section 4.3 that the balanced solutions (31) show good agreement with the exact numerical solution in the leading phase but fail to capture the oscillatory behaviour in the trailing phase. Having derived the wave like WKBJ solutions of the homogeneous wave equations, i.e. (52), (57a) and (57b), we are now in a position to determine whether they correctly describe this oscillatory behaviour.

In Fig. 4 we compare the exact numerical solution to the example problem already discussed in Section 4.3 with the full asymptotic solution, i.e. the sum of the balanced and the WKBJ solution, in the trailing phase ( $\tau > 0$ ). We believe it is fair to say that the full asymptotic solutions approximate the numerical solutions strikingly well. Beyond  $\tau = 2$  the asymptotic solutions are virtually indistinguishable from the numerical solutions. Remarkably, this is so even though for this example we have chosen a shearing wave with an intermediate azimuthal wave number of  $k_y c = \kappa$  for which the ‘small’ parameter  $\epsilon$  attains its maximum value,  $\epsilon = 3/4$  in the case of Keplerian shear considered here, and we are therefore as far away as possible from the asymptotic limit  $\epsilon \ll 1$ .

We note that in the case of  $\hat{p}_y$  there is a small but noticeable discrepancy between the numerical solution and the full asymptotic solution obtained directly from (52). However, we can derive an alternative expression for  $\hat{p}_y$  from PPV conservation. Because the WKBJ solutions are solutions to the free wave equations they should carry no PPV, from which it follows that

$$\tilde{p}_y = \frac{ik_y \tilde{p}_x + (2-q)\Omega \tilde{\rho}}{ik_x} \quad (58)$$

This expression agrees with (52) in the limit  $\epsilon \ll 1$  and we see from Fig. 4 that (58) is in fact more accurate for  $\epsilon \sim 1$ .

We comment that after we have reintroduced the spatial dependence by multiplying with  $\exp(i\vec{k} \cdot \vec{x})$  and then taking the real part, these solutions are found to consist of two waves of equal amplitude travelling in opposite directions. This is a natural outcome given the symmetries of the shearing box. However, for the same reason, both waves transport angular momentum in the same direction, i.e. outward if they are trailing, see Section 4.11.

#### 4.10 Asymptotic behaviour of the WKBJ solutions

The WKBJ solutions for  $\tilde{\rho}$  and  $\tilde{p}_x$  given by (57a) and (57b), respectively, involve complex phases which disguises their large time asymptotic behaviour. To make this more apparent we note that for large times or equivalently  $\tau$  we have

$$\Phi_+ \sim \Phi + i\epsilon \left[ \frac{1}{2} + \ln(2\tau) \right] - \frac{(1+2i\epsilon) \ln(1+2i\epsilon)}{4},$$

where  $\Phi$  is given by equation (51) and is purely real. We see that the imaginary part of  $\Phi_+$  will result in an extra power of  $\tau$  when taking the exponential. This has the consequence that when the sine of the WKBJ phase in (57a) and (57b) is re-expressed in terms of exponentials only those with absolute values that increase with  $\tau$  need to be retained. In this case these are  $\propto \exp(-i\Phi_+/\epsilon)$  and their asymptotic form is given by

$$\exp(-i\Phi_+/\epsilon) \sim 2\tau \exp(-i\Phi/\epsilon) \frac{1}{\sqrt{1+2i\epsilon}} \exp \left[ \frac{1}{2} - \frac{\ln(1+2i\epsilon)}{4i\epsilon} \right],$$

from which it follows that

$$\sin \left( \int_0^t \omega_+ dt' \right) \sim i \left( \frac{\omega}{\Omega} \right) \exp \left( -i \int_0^t \omega dt' \right) \frac{\mathcal{B}_+}{\mathcal{A}_+},$$

where we have defined

$$\mathcal{B}_+ = \frac{\Omega \mathcal{A}_+}{\sqrt{k_y^2 c^2 + \kappa^2 + 2q\Omega i k_y c}} \exp \left[ \frac{1}{2} - \frac{\ln(1 + 2i\epsilon)}{4i\epsilon} \right]. \quad (59)$$

Using the above relations we can readily find the large  $\tau$  asymptotic forms of  $\tilde{\rho}$  and  $\tilde{p}_x$  given by

$$\tilde{\rho} \sim -\hat{\zeta}_s \Omega^{-1} |\mathcal{B}_+| \sqrt{\omega/\Omega} \cos \left( \int_0^t \omega dt' - \text{ph } \mathcal{B}_+ \right) \quad (60a)$$

and

$$\tilde{p}_x \sim i\hat{\zeta}_s H |\mathcal{B}_+| \sqrt{\omega/\Omega} \sin \left( \int_0^t \omega dt' - \text{ph } \mathcal{B}_+ \right). \quad (60b)$$

We thus see that because the WKBJ amplitudes for  $\tilde{\rho}$  and  $\tilde{p}_x$  are complex valued, see (56), the envelope of the oscillation grows in time and there is non-trivial phase shift with respect to  $\tilde{p}_y$ .

#### 4.11 The angular momentum flux

In section 3.2 we obtained two equivalent expressions for the radial angular momentum flux  $F_x$  which uses the radial Lagrangian displacement and  $F'_x$  which uses the  $y$ -component of the momentum density. We determined the angular momentum flux for a single pair of (complex conjugate) shearing waves. Here, we are interested in the angular momentum flux associated with the excited waves, i.e. with the WKBJ solutions. In (20) and (21) we therefore replace  $\hat{\rho}$ ,  $\hat{p}_y$ ,  $\hat{\xi}_x$  by  $\tilde{\rho}$ ,  $\tilde{p}_y$ ,  $\tilde{\xi}_x$ , respectively, and obtain

$$\langle F_x \rangle_{yz} = -2k_y c^2 \text{Im}(\tilde{\xi}_x^* \tilde{\rho}) \quad (61)$$

and

$$\langle F'_x \rangle_{yz} = \frac{2k_y c^2}{(2-q)\Omega\rho_0} \text{Im}(\tilde{p}_y^* \tilde{\rho}), \quad (62)$$

where  $k_y > 0$  is understood.

We can use the WKBJ solutions just obtained to determine these angular momentum fluxes. In order to calculate (61) we need an explicit expression for the radial Lagrangian displacement which in Fourier space is given by

$$\hat{\xi}_x = \frac{1}{\rho_0} \int \hat{p}_x dt.$$

the leading order WKBJ solution in the limit of large  $\tau$  can be calculated from (60b) directly and is given by

$$\tilde{\xi}_x \sim -\frac{i\hat{\zeta}_s H}{\Omega\rho_0} \sqrt{\Omega/\omega} |\mathcal{B}_+| \cos \left( \int_0^t \omega dt' - \text{ph } \mathcal{B}_+ \right)$$

Using this result together with (60a) we readily obtain

$$\lim_{\tau \rightarrow \infty} \overline{\langle F_x \rangle_{yz}} = \frac{k_y c |\hat{\zeta}_s|^2 H^2 |\mathcal{B}_+|^2}{\Omega\rho_0}.$$

With the help of (56) and (59) this may be expressed in the form

$$\lim_{\tau \rightarrow \infty} \overline{\langle F_x \rangle_{yz}} = \frac{2\pi |\hat{\zeta}_s|^2 H^2}{q\rho_0} \frac{\Omega(k_y^2 c^2 + 4\Omega^2) e^{f(\epsilon)} e^{-\pi/2\epsilon}}{[(k_y^2 c^2 + \kappa^2)^2 + (2q\Omega k_y c)^2]^{3/4}}, \quad (63)$$

where the overline denotes an average over one oscillation period, and we have defined

$$f(\epsilon) = 1 - \frac{\tan^{-1}(2\epsilon)}{2\epsilon}.$$

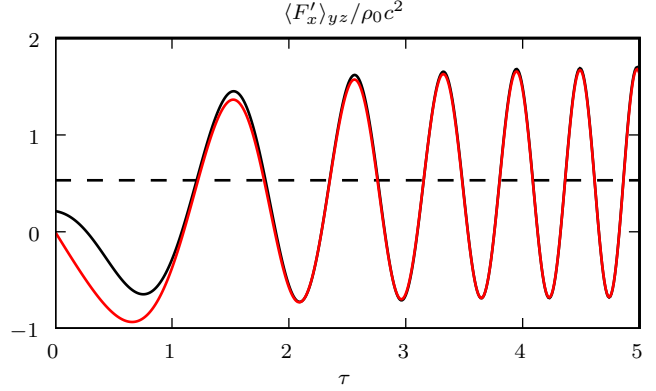


**Figure 5.** Wave action for the wave shown in Fig. 4. The black and red line are the wave action for the wave part of the numerical and WKBJ solution, respectively. The dashed line indicates the large- $\tau$  average value (63).

Alternatively, we may use equation (62) to determine the wave action. This involves  $\tilde{p}_y$  instead of  $\tilde{\xi}_x$  and is accordingly easier to work with in an Eulerian formulation. The calculation of (62) is cumbersome if we use the ‘direct’ WKBJ solution for  $\hat{p}_y$ , given by (52), because its non-trivially phase shifted with respect to the WKBJ solutions for  $\hat{\rho}$  and  $\hat{p}_x$ , given by (57a) and (57b), making the temporal average over one oscillation period somewhat ill defined. However, if we exploit PPV conservation and express  $\hat{p}_y$  in terms of  $\hat{\rho}$  and  $\hat{p}_x$ , see (58), which is also found to be more accurate for  $\epsilon \sim 1$  (see Fig. 4), the calculation is trivial and we obtain

$$\lim_{\tau \rightarrow \infty} \overline{\langle F'_x \rangle_{yz}} = \lim_{\tau \rightarrow \infty} \overline{\langle F_x \rangle_{yz}}. \quad (64)$$

In Fig. 5 we show the angular momentum flux  $\langle F'_x \rangle_{yz}$  associated with the wave parts of solutions plotted in Fig. 4. In order to obtain the wave part of the numerical solution we have simply subtracted the balanced solution.

As expected, the WKBJ solutions agrees with the numerical solution remarkably well. Due to interference between the forward and the backwards travelling waves actually obtained in our numerical solution, the quantity defined by (62) oscillates. However, the average over one oscillation period approaches a constant non-zero value as is expected for a linear wave.

## 5 DISCUSSION

In this paper we have developed a theory of IA wave excitation in a shearing flow with turbulence which may result from the magneto-rotational instability but under the assumption that the magnetic field is too weak to affect the form of the waves significantly. We considered the commonly adopted shearing box model for which the flow was subject the boundary condition of periodicity in shearing coordinates (Goldreich & Lynden-Bell 1965). The excitation mechanism has similarities to Lighthill’s theory of noise generation by turbulence (Lighthill 1952) but with modifications to take account of rotation and shear.

The main feature resulting from the shear is that wave excitation occurs through a sequence of regularly spaced

swings as the wave changes from leading to trailing form. For a fixed azimuthal wave number  $k_y$ , and a Keplerian rotation profile, the swings are separated by a time interval  $\delta t_s = T_{\text{orb}}/(qk_y L_x)$ , where the orbital period  $T_{\text{orb}} = 2\pi/\Omega$ . For the optimal azimuthal wave number  $k_y = 1/H$  (see discussion below) and  $L_x = H$  as an estimated radial correlation length of the turbulence, which should also be the minimum box size required to capture its essential properties, it follows that  $\delta t_s \approx T_{\text{orb}}$ .

The wave equations governing the excitation during a particular swing were found to depend on time alone and under the assumption that the important source terms causing the wave excitation are associated with the pseudo potential vorticity, they could be solved to find the asymptotic wave form and net positive wave action produced. The form of the wave equations necessitated a WKBJ analysis that had to be extended into the complex plane. In this respect the formalism differs from shearing box analyses that adopt rigid or free boundary conditions, or which assume strictly harmonic forcing with radial boundaries extended to infinity, rather than periodicity in shearing coordinates. In the former cases one can separate out a harmonic time dependence and solve a problem in space for the wave amplitude (e.g. Narayan et al. 1987).

The analysis of the wave excitation process driven by pseudo potential vorticity carried out in this paper has similarities to an analysis of Inertia-Gravity waves excited in the earth's atmosphere or oceans by Vanneste & Yavneh (2004) who adopt a potential vorticity source and perform a similar WKBJ analysis in the complex plane.

The excitation process produces waves of equal amplitude propagating in opposite directions. As these waves are both trailing, by symmetry each produces an equal outward angular momentum flow. Even when the excitation process is linear, as the waves propagate away, the radial wave length is expected to shorten until shock dissipation eventually occurs (e.g. Goodman & Rafikov 2001). Thus waves are always likely to be seen to manifest non-linear effects although the characteristic radial wave length is likely to shorten as the strength of the excitation process decreases. When waves behave linearly during the initial excitation, but still undergo significant but not complete dissipation between successive swings, the rate of angular momentum transport can be estimated as the wave action produced in single swing given by equation (63). This situation is found to occur in the simulations presented in paper II.

An important quantity is the value of the azimuthal/horizontal wave number,  $k_y$ , for which the wave excitation is most favoured, which we define as being value for which the wave action produced is maximal. Equation (63) indicates that this action is a product of a known function of  $k_y$  and the square of the appropriate source Fourier amplitude, at the time of swing, which can be determined from the PPV. The latter quantity, being determined by the non linear hydromagnetic turbulence cannot be determined from the wave excitation calculations performed here. This aspect is discussed in paper II where relevant numerical simulations are performed and analysed. Here we shall anticipate results and assume that the PPV spectrum is relatively flat at small  $k_y$  with the consequence that the dependence of the wave action on  $k_y$  is determined by the factor in equation (63)

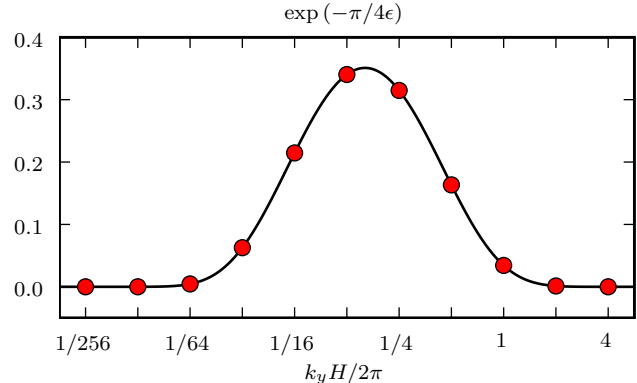


**Figure 6.** Exponential dependence of the WKBJ amplitudes on the azimuthal wave number  $k_y$  for a Keplerian rotation law.

that is determined solely by the WKBJ theory presented here.

The wave amplitude depends on the azimuthal wave number  $k_y$  through the parameter

$$\epsilon = \frac{q\Omega k_y c}{k_y^2 c^2 + \kappa^2}$$

in such a way that it is exponentially small for  $\epsilon \ll 1$ , see e.g. (53). Given the fact that  $\epsilon$  is small both in the small and the long azimuthal wave number limit, we deduce that wave excitation will be most effective near the optimal wave number

$$k_y^{\text{opt}} = \kappa/c$$

for which  $\epsilon$  takes its maximum value

$$\epsilon_{\text{max}} = q\Omega/2\kappa.$$

For a Keplerian disc with  $q = 3/2$  and  $\kappa = 1$  we have  $k_y^{\text{opt}} = 1/H$  and thus  $\epsilon_{\text{max}} = 3/4$ . We recall that WKBJ theory gives very accurate results for values of  $\epsilon$  as large as this. For illustrative purposes we plot the exponential dependence of the wave amplitudes as a function of azimuthal wave number in Fig. 6. We see that amplitude of the excited wave falls off rapidly away from the optimal wave number.

The arguments given above suggest that IA wave production will be most effective for  $k_y \sim k_y^{\text{opt}}$ . This is the longest possible azimuthal wave length for a box with  $L_y = 2\pi H$  as is commonly adopted. For boxes of this size and smaller wave production is expected to be most effective at the longest azimuthal wave length. On the other hand once  $L_y$  exceeds  $2\pi H$  the longest wave length is expected to no longer be the most effective. This is fully supported by the simulation results presented in paper II. In this paper we confirm the main features of the excitation process described here and verify the dominance of the pseudo potential vorticity related source terms. Although the waves are observed to become non linear very soon after the initial excitation phase, the main features of the analysis presented here are confirmed. This suggests that future useful extensions can be made to the analysis of wave excitation under more general conditions such as those that incorporate significant self-gravity. We plan to undertake these in the near future.

## ACKNOWLEDGEMENTS

T. H. acknowledges support from the STFC and the Isaac Newton Trust. The authors wish to thank Stephen J. Cowley and James C. McWilliams for rewarding discussions.

## REFERENCES

- Armitage P. J., 1998, *ApJ*, 501, L189+
- Balbus S. A., Hawley J. F., 1991, *ApJ*, 376, 214
- Balbus S. A., Hawley J. F., 1998, *Reviews of Modern Physics*, 70, 1
- Fromang S., Papaloizou J., 2007, *A&A*, 468, 1
- Gardiner T. A., Stone J. M., 2006, in Zank G. P., Pogorelov N. V., eds, *Numerical Modeling of Space Plasma Flows* Vol. 359 of *Astronomical Society of the Pacific Conference Series*, Multidimensional MHD Algorithms in Athena. pp 143–+
- Goldreich P., Lynden-Bell D., 1965, *MNRAS*, 130, 125
- Goodman J., Rafikov R. R., 2001, *ApJ*, 552, 793
- Johnson B. M., Gammie C. F., 2005, *ApJ*, 626, 978
- Lighthill M. J., 1952, *Royal Society of London Proceedings Series A*, 211, 564
- Lin D. N. C., Papaloizou J. C. B., 1996, *ARA&A*, 34, 703
- Narayan R., Goldreich P., Goodman J., 1987, *MNRAS*, 228, 1
- Nelson R. P., 2005, *A&A*, 443, 1067
- Nelson R. P., Papaloizou J. C. B., 2004, *MNRAS*, 350, 849
- Papaloizou J. C. B., Lin D. N. C., 1995, *ARA&A*, 33, 505
- Shakura N. I., Syunyaev R. A., 1973, *A&A*, 24, 337
- Thomson W., 1887, *Philos. Mag*, 24, 188
- Vanneste J., Yavneh I., 2004, *Journal of Atmospheric Sciences*, 61, 211